

Test of lepton flavor universality and search for lepton flavor violation in $B \rightarrow K\ell\ell$ decays

The Belle Collaboration

S. Choudhury,²⁴ S. Sandilya,^{7,24} K. Trabelsi,⁴³ A. Giri,²⁴ H. Aihara,⁹² S. Al Said,^{85,37} D. M. Asner,³ H. Atmacan,⁷ V. Aulchenko,^{4,67} T. Aushev,¹⁹ R. Ayad,⁸⁵ V. Babu,⁸ S. Bahinipati,²³ P. Behera,²⁵ C. Beleño,¹² K. Belous,²⁸ J. Bennett,⁵³ F. Bernlochner,² M. Bessner,¹⁶ V. Bhardwaj,²² T. Bilka,⁵ J. Biswal,³³ G. Bonvicini,⁹⁷ A. Bozek,⁶³ M. Bračko,^{50,33} T. E. Browder,¹⁶ M. Campajola,^{30,58} D. Červenkov,⁵ M.-C. Chang,¹⁰ P. Chang,⁶² V. Chekelian,⁵¹ A. Chen,⁶⁰ B. G. Cheon,¹⁵ K. Chilikin,⁴⁴ K. Cho,³⁸ S.-K. Choi,¹⁴ Y. Choi,⁸³ D. Cinabro,⁹⁷ S. Cunliffe,⁸ N. Dash,²⁵ G. De Nardo,^{30,58} R. Dhamija,²⁴ F. Di Capua,^{30,58} J. Dingfelder,² Z. Doležal,⁵ T. V. Dong,¹¹ D. Dossett,⁵² S. Dubey,¹⁶ S. Eidelman,^{4,67,44} D. Epifanov,^{4,67} T. Ferber,⁸ D. Ferlewicz,⁵² B. G. Fulsom,⁷⁰ R. Garg,⁷¹ V. Gaur,⁹⁶ N. Gabyshev,^{4,67} A. Garmash,^{4,67} P. Goldenzweig,³⁴ B. Golob,^{46,33} D. Greenwald,⁸⁷ C. Hadjivasiliou,⁷⁰ O. Hartbrich,¹⁶ H. Hayashii,⁵⁹ M. T. Hedges,¹⁶ M. Hernandez Villanueva,⁵³ T. Higuchi,³⁵ W.-S. Hou,⁶² C.-L. Hsu,⁸⁴ T. Iijima,^{57,56} K. Inami,⁵⁶ A. Ishikawa,^{17,13} R. Itoh,^{17,13} M. Iwasaki,⁶⁸ Y. Iwasaki,¹⁷ W. W. Jacobs,²⁶ E.-J. Jang,¹⁴ H. B. Jeon,⁴² S. Jia,¹¹ Y. Jin,⁹² C. W. Joo,³⁵ K. K. Joo,⁶ J. Kahn,³⁴ A. B. Kaliyar,⁸⁶ K. H. Kang,⁴² G. Karyan,⁸ H. Kichimi,¹⁷ C. Kiesling,⁵¹ B. H. Kim,⁷⁹ D. Y. Kim,⁸² K.-H. Kim,⁹⁹ K. T. Kim,³⁹ S. H. Kim,⁷⁹ Y.-K. Kim,⁹⁹ K. Kinoshita,⁷ P. Kodyš,⁵ S. Korpar,^{50,33} D. Kotchetkov,¹⁶ P. Krizan,^{46,33} R. Kroeger,⁵³ P. Krokovny,^{4,67} T. Kuhr,⁴⁷ R. Kulasiri,³⁶ R. Kumar,⁷⁴ K. Kumara,⁹⁷ A. Kuzmin,^{4,67} Y.-J. Kwon,⁹⁹ K. Lalwani,⁴⁹ S. C. Lee,⁴² P. Lewis,² C. H. Li,⁴⁵ L. K. Li,⁷ Y. B. Li,⁷² L. Li Gioi,⁵¹ J. Libby,²⁵ K. Lieret,⁴⁷ Z. Liptak,^{† 16} D. Liventsev,^{97,17} T. Luo,¹¹ M. Masuda,^{91,75} T. Matsuda,⁵⁴ D. Matvienko,^{4,67,44} M. Merola,^{30,58} K. Miyabayashi,⁵⁹ R. Mizuk,^{44,19} G. B. Mohanty,⁸⁶ S. Mohanty,^{86,95} T. J. Moon,⁷⁹ T. Mori,⁵⁶ I. Nakamura,^{17,13} K. R. Nakamura,¹⁷ M. Nakao,^{17,13} Z. Natkaniec,⁶³ A. Natochii,¹⁶ L. Nayak,²⁴ M. Nayak,⁸⁸ M. Niiyama,⁴⁰ N. K. Nisar,³ S. Nishida,^{17,13} K. Ogawa,⁶⁵ H. Ono,^{64,65} Y. Onuki,⁹² P. Oskin,⁴⁴ P. Pakhlov,^{44,55} G. Pakhlova,^{19,44} S. Pardi,³⁰ H. Park,⁴² S.-H. Park,⁹⁹ S. Patra,²² S. Paul,^{87,51} T. K. Pedlar,⁴⁸ R. Pestotnik,³³ L. E. Piilonen,⁹⁶ T. Podobnik,^{46,33} V. Popov,¹⁹ E. Prencipe,²⁰ M. T. Prim,³⁴ A. Rabusov,⁸⁷ A. Rostomyan,⁸ N. Rout,²⁵ M. Rozanska,⁶³ G. Russo,⁵⁸ D. Sahoo,⁸⁶ Y. Sakai,^{17,13} L. Santelj,^{46,33} T. Sanuki,⁹⁰ V. Savinov,⁷³ G. Schnell,^{1,21} J. Schueler,¹⁶

[†]now at Hiroshima University.

C. Schwanda,²⁹ A. J. Schwartz,⁷ Y. Seino,⁶⁵ K. Senyo,⁹⁸ M. E. Sevier,⁵²
M. Shapkin,²⁸ V. Shebalin,¹⁶ J.-G. Shiu,⁶² B. Shwartz,^{4,67} F. Simon,⁵¹ A. Sokolov,²⁸
E. Solovieva,⁴⁴ S. Stanič,⁶⁶ M. Starič,³³ Z. S. Stottler,⁹⁶ T. Sumiyoshi,⁹⁴
W. Sutcliffe,² M. Takizawa,^{80,18,76} U. Tamponi,³¹ K. Tanida,³² F. Tenchini,⁸
M. Uchida,⁹³ S. Uehara,^{17,13} T. Uglov,^{44,19} Y. Unno,¹⁵ S. Uno,^{17,13} P. Urquijo,⁵²
Y. Ushiroda,^{17,13} R. Van Tonder,² G. Varner,¹⁶ K. E. Varvell,⁸⁴ A. Vinokurova,^{4,67}
V. Vorobyev,^{4,67,44} E. Waheed,¹⁷ C. H. Wang,⁶¹ E. Wang,⁷³ M.-Z. Wang,⁶²
P. Wang,²⁷ M. Watanabe,⁶⁵ S. Watanuki,⁴³ S. Wehle,⁸ J. Wiechczynski,⁶³ E. Won,³⁹
X. Xu,⁸¹ B. D. Yabsley,⁸⁴ W. Yan,⁷⁸ S. B. Yang,³⁹ H. Ye,⁸ J. Yelton,⁹ J. H. Yin,³⁹
C. Z. Yuan,²⁷ Y. Yusa,⁶⁵ Z. P. Zhang,⁷⁸ V. Zhilich,^{4,67} V. Zhukova⁴⁴

¹ *University of the Basque Country UPV/EHU, 48080 Bilbao, Spain*

² *University of Bonn, 53115 Bonn, Germany*

³ *Brookhaven National Laboratory, Upton, New York 11973, USA*

⁴ *Budker Institute of Nuclear Physics SB RAS, Novosibirsk 630090, Russian Federation*

⁵ *Faculty of Mathematics and Physics, Charles University, 121 16 Prague, The Czech Republic*

⁶ *Chonnam National University, Gwangju 61186, South Korea*

⁷ *University of Cincinnati, Cincinnati, OH 45221, USA*

⁸ *Deutsches Elektronen-Synchrotron, 22607 Hamburg, Germany*

⁹ *University of Florida, Gainesville, FL 32611, USA*

¹⁰ *Department of Physics, Fu Jen Catholic University, Taipei 24205, Taiwan*

¹¹ *Key Laboratory of Nuclear Physics and Ion-beam Application (MOE) and Institute of Modern Physics, Fudan University, Shanghai 200443, PR China*

¹² *II. Physikalisches Institut, Georg-August-Universität Göttingen, 37073 Göttingen, Germany*

¹³ *SOKENDAI (The Graduate University for Advanced Studies), Hayama 240-0193, Japan*

¹⁴ *Gyeongsang National University, Jinju 52828, South Korea*

¹⁵ *Department of Physics and Institute of Natural Sciences, Hanyang University, Seoul 04763, South Korea*

¹⁶ *University of Hawaii, Honolulu, HI 96822, USA*

¹⁷ *High Energy Accelerator Research Organization (KEK), Tsukuba 305-0801, Japan*

¹⁸ *J-PARC Branch, KEK Theory Center, High Energy Accelerator Research Organization (KEK), Tsukuba 305-0801, Japan*

¹⁹ *Higher School of Economics (HSE), Moscow 101000, Russian Federation*

²⁰ *Forschungszentrum Jülich, 52425 Jülich, Germany*

²¹ *IKERBASQUE, Basque Foundation for Science, 48013 Bilbao, Spain*

²² *Indian Institute of Science Education and Research Mohali, SAS Nagar, 140306, India*

²³ *Indian Institute of Technology Bhubaneswar, Satya Nagar 751007, India*

²⁴ *Indian Institute of Technology Hyderabad, Telangana 502285, India*

²⁵ *Indian Institute of Technology Madras, Chennai 600036, India*

²⁶ *Indiana University, Bloomington, IN 47408, USA*

²⁷ *Institute of High Energy Physics, Chinese Academy of Sciences, Beijing 100049, PR China*

²⁸ *Institute for High Energy Physics, Protvino 142281, Russian Federation*

²⁹ *Institute of High Energy Physics, Vienna 1050, Austria*

³⁰ *INFN - Sezione di Napoli, 80126 Napoli, Italy*

³¹ *INFN - Sezione di Torino, 10125 Torino, Italy*

- ³²Advanced Science Research Center, Japan Atomic Energy Agency, Naka 319-1195, Japan
- ³³J. Stefan Institute, 1000 Ljubljana, Slovenia
- ³⁴Institut für Experimentelle Teilchenphysik, Karlsruher Institut für Technologie, 76131 Karlsruhe, Germany
- ³⁵Kavli Institute for the Physics and Mathematics of the Universe (WPI), University of Tokyo, Kashiwa 277-8583, Japan
- ³⁶Kennesaw State University, Kennesaw GA 30144, USA
- ³⁷Department of Physics, Faculty of Science, King Abdulaziz University, Jeddah 21589, Saudi Arabia
- ³⁸Korea Institute of Science and Technology Information, Daejeon 34141, South Korea
- ³⁹Korea University, Seoul 02841, South Korea
- ⁴⁰Kyoto Sangyo University, Kyoto 603-8555, Japan
- ⁴¹Kyoto University, Kyoto 606-8502, Japan
- ⁴²Kyungpook National University, Daegu 41566, South Korea
- ⁴³Université Paris-Saclay, CNRS/IN2P3, IJCLab, 91405 Orsay, France
- ⁴⁴P.N. Lebedev Physical Institute of the Russian Academy of Sciences, Moscow 119991, Russian Federation
- ⁴⁵Liaoning Normal University, Dalian 116029, China
- ⁴⁶Faculty of Mathematics and Physics, University of Ljubljana, 1000 Ljubljana, Slovenia
- ⁴⁷Ludwig Maximilians University, 80539 Munich, Germany
- ⁴⁸Luther College, Decorah, IA 52101, USA
- ⁴⁹Malaviya National Institute of Technology Jaipur, Jaipur 302017, India
- ⁵⁰University of Maribor, 2000 Maribor, Slovenia
- ⁵¹Max-Planck-Institut für Physik, 80805 München, Germany
- ⁵²School of Physics, University of Melbourne, Victoria 3010, Australia
- ⁵³University of Mississippi, University, MS 38677, USA
- ⁵⁴University of Miyazaki, Miyazaki 889-2192, Japan
- ⁵⁵Moscow Physical Engineering Institute, Moscow 115409, Russian Federation
- ⁵⁶Graduate School of Science, Nagoya University, Nagoya 464-8602, Japan
- ⁵⁷Kobayashi-Maskawa Institute, Nagoya University, Nagoya 464-8602, Japan
- ⁵⁸Università di Napoli Federico II, 80126 Napoli, Italy
- ⁵⁹Nara Women's University, Nara 630-8506, Japan
- ⁶⁰National Central University, Chung-li 32054, Taiwan
- ⁶¹National United University, Miao Li 36003, Taiwan
- ⁶²Department of Physics, National Taiwan University, Taipei 10617, Taiwan
- ⁶³H. Niewodniczanski Institute of Nuclear Physics, Krakow 31-342, Poland
- ⁶⁴Nippon Dental University, Niigata 951-8580, Japan
- ⁶⁵Niigata University, Niigata 950-2181, Japan
- ⁶⁶University of Nova Gorica, 5000 Nova Gorica, Slovenia
- ⁶⁷Novosibirsk State University, Novosibirsk 630090, Russian Federation
- ⁶⁸Osaka City University, Osaka 558-8585, Japan
- ⁶⁹Osaka University, Osaka 565-0871, Japan
- ⁷⁰Pacific Northwest National Laboratory, Richland, WA 99352, USA
- ⁷¹Panjab University, Chandigarh 160014, India

- ⁷²*Peking University, Beijing 100871, PR China*
- ⁷³*University of Pittsburgh, Pittsburgh, PA 15260, USA*
- ⁷⁴*Punjab Agricultural University, Ludhiana 141004, India*
- ⁷⁵*Research Center for Nuclear Physics, Osaka University, Osaka 567-0047, Japan*
- ⁷⁶*Meson Science Laboratory, Cluster for Pioneering Research, RIKEN, Saitama 351-0198, Japan*
- ⁷⁷*Theoretical Research Division, Nishina Center, RIKEN, Saitama 351-0198, Japan*
- ⁷⁸*Department of Modern Physics and State Key Laboratory of Particle Detection and Electronics, University of Science and Technology of China, Hefei 230026, PR China*
- ⁷⁹*Seoul National University, Seoul 08826, South Korea*
- ⁸⁰*Showa Pharmaceutical University, Tokyo 194-8543, Japan*
- ⁸¹*Soochow University, Suzhou 215006, China*
- ⁸²*Soongsil University, Seoul 06978, South Korea*
- ⁸³*Sungkyunkwan University, Suwon 16419, South Korea*
- ⁸⁴*School of Physics, University of Sydney, New South Wales 2006, Australia*
- ⁸⁵*Department of Physics, Faculty of Science, University of Tabuk, Tabuk 71451, Saudi Arabia*
- ⁸⁶*Tata Institute of Fundamental Research, Mumbai 400005, India*
- ⁸⁷*Department of Physics, Technische Universität München, 85748 Garching, Germany*
- ⁸⁸*School of Physics and Astronomy, Tel Aviv University, Tel Aviv 69978, Israel*
- ⁸⁹*Toho University, Funabashi 274-8510, Japan*
- ⁹⁰*Department of Physics, Tohoku University, Sendai 980-8578, Japan*
- ⁹¹*Earthquake Research Institute, University of Tokyo, Tokyo 113-0032, Japan*
- ⁹²*Department of Physics, University of Tokyo, Tokyo 113-0033, Japan*
- ⁹³*Tokyo Institute of Technology, Tokyo 152-8550, Japan*
- ⁹⁴*Tokyo Metropolitan University, Tokyo 192-0397, Japan*
- ⁹⁵*Utkal University, Bhubaneswar 751004, India*
- ⁹⁶*Virginia Polytechnic Institute and State University, Blacksburg, VA 24061, USA*
- ⁹⁷*Wayne State University, Detroit, MI 48202, USA*
- ⁹⁸*Yamagata University, Yamagata 990-8560, Japan*
- ⁹⁹*Yonsei University, Seoul 03722, South Korea*

ABSTRACT: We present measurements of the branching fractions for the decays $B \rightarrow K\mu^+\mu^-$ and $B \rightarrow Ke^+e^-$, and their ratio (R_K), using a data sample of 711 fb^{-1} that contains $772 \times 10^6 \text{ } B\bar{B}$ events. The data were collected at the $\Upsilon(4S)$ resonance with the Belle detector at the KEKB asymmetric-energy e^+e^- collider. The ratio R_K is measured in five bins of dilepton invariant-mass-squared (q^2): $q^2 \in (0.1, 4.0), (4.0, 8.12), (1.0, 6.0), (10.2, 12.8)$ and $(> 14.18) \text{ GeV}^2/c^4$, along with the whole q^2 region. The R_K value for $q^2 \in (1.0, 6.0) \text{ GeV}^2/c^4$ is $1.03^{+0.28}_{-0.24} \pm 0.01$. The first and second uncertainties listed are statistical and systematic, respectively. All results for R_K are consistent with Standard Model predictions. We also measure CP -averaged isospin asymmetries in the same q^2 bins. The results are consistent with a null asymmetry, with the largest difference of 2.6 standard deviations occurring for the $q^2 \in (1.0, 6.0) \text{ GeV}^2/c^4$ bin in the mode with muon final states. The measured differential branching fractions, $d\mathcal{B}/dq^2$, are consistent with theoretical predictions for charged B decays, while the corresponding values are below the expectations for neutral B decays. We have also searched for lepton-flavor-violating $B \rightarrow K\mu^\pm e^\mp$ decays and set 90% confidence-level upper limits on the branching fraction in the range of 10^{-8} for $B^+ \rightarrow K^+\mu^\pm e^\mp$, and $B^0 \rightarrow K^0\mu^\pm e^\mp$ modes.

Contents

1	Introduction	1
2	Data samples and Belle detector	2
3	Analysis Overview	2
4	Results	6
5	Systematic uncertainties	14
6	Summary	15
7	Acknowledgments	16

1 Introduction

The decays $B \rightarrow K\ell^+\ell^-$ ($\ell = e, \mu$), mediated by the $b \rightarrow s\ell^+\ell^-$ quark-level transition, constitute a flavor-changing neutral current process. Such processes are forbidden at tree level in the Standard Model (SM) but can proceed via suppressed loop-level diagrams, and they are therefore sensitive to particles predicted in a number of new physics models [1, 2]. A robust observable [3] to test the SM prediction is the lepton-flavor-universality (LFU) ratio,

$$R_H = \frac{\int \frac{d\Gamma}{dq^2}[B \rightarrow H\mu^+\mu^-]dq^2}{\int \frac{d\Gamma}{dq^2}[B \rightarrow He^+e^-]dq^2}, \quad (1.1)$$

where H is a K or K^* meson and the decay rate Γ is integrated over a range of the dilepton invariant mass squared, $q^2 \equiv M^2(\ell^+\ell^-)$. For R_{K^*} , recently LHCb [4] reported hints of deviations from SM expectations, while Belle [5] results are consistent with the SM with relatively larger uncertainties. LHCb also measured R_K [6], reporting a difference of about 2.5 standard deviations (σ) from the SM prediction in the $q^2 \in (1.1, 6.0) \text{ GeV}^2/c^4$ bin. A previous measurement of the same quantity was performed by Belle [7] in the whole q^2 range with a data sample of $657 \times 10^6 B\bar{B}$ events. The result presented here is obtained from a multidimensional fit performed on the full Belle data sample of $772 \times 10^6 B\bar{B}$ events, and supersedes our previous result [7].

Another theoretically robust observable [8], where the dominant form-factor-related uncertainties also cancel, is the CP -averaged isospin asymmetry, representing the difference in partial widths:

$$A_I = \frac{(\tau_{B^+}/\tau_{B^0})\mathcal{B}(B^0 \rightarrow K^0\ell^+\ell^-) - \mathcal{B}(B^+ \rightarrow K^+\ell^+\ell^-)}{(\tau_{B^+}/\tau_{B^0})\mathcal{B}(B^0 \rightarrow K^0\ell^+\ell^-) + \mathcal{B}(B^+ \rightarrow K^+\ell^+\ell^-)}, \quad (1.2)$$

where $\tau_{B^+}/\tau_{B^0} = 1.076 \pm 0.004$ is the lifetime ratio of B^+ to B^0 [9]. The A_I value is expected to be close to zero in the SM [10]. Earlier, BaBar [11] and Belle [7] reported A_I to be significantly below zero, especially in the q^2 region below the J/ψ resonance, while LHCb [12] reported results consistent with SM predictions.

In many theoretical models, lepton flavor violation (LFV) accompanies LFU violation [13]. With neutrino mixing, LFV is only possible at rates far below the current experimental sensitivity. In case of signal, this will signify physics beyond SM [14]. The LFV in B decays can be studied via $B \rightarrow K\mu^\pm e^\mp$. The most stringent upper limits on $B^+ \rightarrow K^+\mu^+e^-$ and $B^+ \rightarrow K^+\mu^-e^+$ set by LHCb [15] are 6.4×10^{-9} and 7.0×10^{-9} at 90% confidence level (CL). Prior to that, $B^0 \rightarrow K^0\mu^\pm e^\mp$ decays were searched for by BaBar [16], which set a 90% CL upper limit on the branching fraction of 2.7×10^{-7} .

In this paper, we report a measurement of the decay branching fractions of $B \rightarrow K\ell^+\ell^-$, R_K and A_I in the whole q^2 range as well as in five q^2 bins [(0.1, 4.0), (4.0, 8.12), (1.0, 6.0), (10.2, 12.8) and (> 14.18)] GeV^2/c^4 . We also search for $B \rightarrow K\mu^\pm e^\mp$ decays using the full Belle data sample.

2 Data samples and Belle detector

This analysis uses a 711 fb^{-1} data sample containing $(772 \pm 11) \times 10^6$ $B\bar{B}$ events, collected at the $\Upsilon(4S)$ resonance by the Belle experiment at the KEKB e^+e^- collider [17]. An 89 fb^{-1} data sample recorded 60 MeV below the $\Upsilon(4S)$ peak (off-resonance) is used to estimate the background contribution from $e^+e^- \rightarrow q\bar{q}$ ($q = u, d, s, c$) continuum events.

The Belle detector [18] is a large-solid-angle magnetic spectrometer composed of a silicon vertex detector (SVD), a 50-layer central drift chamber (CDC), an array of aerogel threshold Cherenkov counters (ACC), a barrel-like arrangement of time-of-flight scintillation counters (TOF), and an electromagnetic calorimeter (ECL) comprising CsI(Tl) crystals. All these subdetectors are located inside a superconducting solenoid coil that provides a 1.5 T magnetic field. An iron flux-return yoke placed outside the coil is instrumented with resistive plate chambers (KLM) to detect K_L^0 mesons and muons. Two inner detector configurations were used: a 2.0 cm radius beam pipe and a three-layer SVD for the first sample of 140 fb^{-1} ; and a 1.5 cm radius beam pipe, a four-layer SVD, and a small-cell inner CDC for the remaining 571 fb^{-1} [19].

To study properties of signal events and optimize selection criteria, we use samples of Monte Carlo (MC) simulated events. The $B \rightarrow K\ell^+\ell^-$ modes are generated with the EVTGEN package [20] based on a model described in Ref. [21], while LFV modes are generated with a phase-space model. The PHOTOS [22] package is used to incorporate final-state radiation. The detector response is simulated with GEANT3 [23].

3 Analysis Overview

We reconstruct $B \rightarrow K\ell^+\ell^-$ ($K = K^+, K_S^0$) [24] decays by selecting charged particles that originate from the vicinity of the e^+e^- interaction point (IP), except for those originating from K_S^0 decays. We require impact parameters less than 1.0 cm in the transverse plane

and less than 4.0 cm along the z axis (parallel to the e^+ beam). To reduce backgrounds from low-momentum particles, we require that tracks have a minimum transverse momentum of $100 \text{ MeV}/c$.

From the list of selected tracks, we identify K^+ candidates using a likelihood ratio $\mathcal{R}_{K/\pi} = \mathcal{L}_K/(\mathcal{L}_K + \mathcal{L}_\pi)$, where \mathcal{L}_K and \mathcal{L}_π are the likelihoods for charged kaons and pions, respectively, calculated based on the number of photoelectrons in the ACC, the specific ionization in the CDC, and the time of flight as determined from the TOF. We select kaons by requiring $\mathcal{R}_{K/\pi} > 0.6$, which has a kaon identification efficiency of 92% and a pion misidentification rate of 7%. For the neutral B decay, candidate K_S^0 mesons are reconstructed by combining two oppositely charged tracks (assumed to be pions) with an invariant mass between 487 and 508 MeV/c^2 ; this corresponds to a 3σ window around the nominal K_S^0 mass [9]. Such candidates are further identified with a neural network (NN). The variables used for this NN are: the K_S^0 momentum; the distance along the z axis between the two track helices at their closest approach; the flight length in the transverse plane; the angle between the K_S^0 momentum and the vector joining the IP with the K_S^0 decay vertex; the angle between the pion momentum and the laboratory-frame direction in the K_S^0 rest frame; the distances-of-closest-approach in the transverse plane between the IP and the two pion helices; and the number of hits in the CDC; and the presence or absence of hits in the SVD for each pion track.

Muon candidates are identified based on information from the KLM. We require that candidates have a momentum greater than 0.8 GeV/c (enabling them to reach the KLM subdetector), and a penetration depth and degree of transverse scattering consistent with those of a muon [25]. The latter information is used to calculate a normalized muon likelihood \mathcal{R}_μ , and we require $\mathcal{R}_\mu > 0.9$. For this requirement, the average muon detection efficiency is 89%, with a pion misidentification rate of 1.5% [26].

Electron candidates are required to have a momentum greater than 0.5 GeV/c and are identified using the ratio of calorimetric cluster energy to the CDC track momentum; the shower shape in the ECL; the matching of the track with the ECL cluster; the specific ionization in the CDC; and the number of photoelectrons in the ACC. This information is used to calculate a normalized electron likelihood \mathcal{R}_e , and we require $\mathcal{R}_e > 0.9$. This requirement has an efficiency of 92% and a pion misidentification rate below 1% [27]. To recover energy loss due to possible bremsstrahlung, we search for photons inside a cone of radius 50 mrad centered around the electron direction. For each photon found within the cone, its four-momentum is added to that of the initial electron.

Charged (neutral) B candidates are reconstructed by combining K^\pm (K_S^0) with suitable μ^\pm or e^\pm candidates. To distinguish signal from background events, two kinematic variables are used: the beam-energy-constrained mass $M_{\text{bc}} = \sqrt{(E_{\text{beam}}/c^2)^2 - (p_B/c)^2}$, and the energy difference $\Delta E = E_B - E_{\text{beam}}$, where E_{beam} is the beam energy, and E_B and p_B are the energy and momentum, respectively, of the B candidate. All these quantities are calculated in the e^+e^- center-of-mass (CM) frame. For signal events, the ΔE distribution peaks at zero, and the M_{bc} distribution peaks near the B mass. We retain candidates satisfying the requirements $-0.10 < \Delta E < 0.25 \text{ GeV}$ and $M_{\text{bc}} > 5.2 \text{ GeV}/c^2$.

With the above selection criteria applied, about 2% of signal MC events are found to

have more than one B candidate. For these events, we retain the candidate with smallest χ^2 value resulting from a vertex fit of the B daughter particles. From MC simulation, this criterion is found to select the correct signal candidate 78-85% of the time, depending on the decay mode. The decays $B \rightarrow J/\psi(\rightarrow \ell^+\ell^-)K$ and $B \rightarrow \psi(2S)(\rightarrow \ell^+\ell^-)K$, used later as control samples, are suppressed in the signal selection via a set of vetoes $8.75 < q^2 < 10.2 \text{ GeV}^2/c^4$ and $13.0 < q^2 < 14.0 \text{ GeV}^2/c^4$ with the dimuon; $8.12 < q^2 < 10.2 \text{ GeV}^2/c^4$ and $12.8 < q^2 < 14.0 \text{ GeV}^2/c^4$ with the dielectron final states for $B \rightarrow J/\psi K$ and $B \rightarrow \psi(2S)K$, respectively. An additional veto of the low q^2 region ($< 0.05 \text{ GeV}^2/c^4$) is applied in the case of $B \rightarrow Ke^+e^-$ to suppress possible contaminations from $\gamma^* \rightarrow e^+e^-$ and $\pi^0 \rightarrow \gamma e^+e^-$.

At this stage of the analysis, there is significant background from continuum processes and other B decays. As lighter quarks are produced with large kinetic energy, the former events tend to consist of two back-to-back jets of pions and kaons. In contrast, $B\bar{B}$ events are produced almost at rest in the CM frame, resulting in more spherically distributed daughter particles. We thus distinguish $B\bar{B}$ events from $q\bar{q}$ background based on event topology.

Background arising from B decays has typically two uncorrelated leptons in the final state. Such background falls into three categories: (a) both B and \bar{B} decay semileptonically; (b) a $B \rightarrow \bar{D}^{(*)}X\ell^+\nu$ decay is followed by $\bar{D}^{(*)} \rightarrow X\ell^-\bar{\nu}$; and (c) hadronic B decays where one or more daughter particles are misidentified as leptons. To suppress continuum as well as $B\bar{B}$ background, we use an NN trained with the following input variables:

1. A likelihood ratio constructed from a set of modified Fox-Wolfram moments [28, 29].
2. The angle θ_B between the B flight direction and the z axis in the CM frame (for $B\bar{B}$ events, $dN/d\cos\theta_B \propto 1 - \cos^2\theta_B$, whereas for continuum events, $dN/d\cos\theta_B \approx$ constant, where N is the number of events).
3. The angle θ_T between the thrust axes calculated from final-state particles for the candidate B and for the rest of the event in the CM frame. (The thrust axis is the direction that maximizes the sum of the longitudinal momenta of the considered particles). For signal events, the $\cos\theta_T$ distribution is flat, whereas for continuum events it peaks near ± 1 .
4. Flavor-tagging information from the tag-side (recoiling) B decay. The flavor-tagging algorithm [30] outputs two variables: the flavor q of the tag-side B , and the tag quality r . The latter ranges from zero for no flavor information to one for an unambiguous flavor assignment.
5. The confidence level of the B vertex fitted from all daughter particles.
6. The separation in z between the signal B decay vertex and that of the other B in the event.
7. The separation between the two leptons along the z -axis divided by the quadratic sum of uncertainties in the z -intercepts of the tracks.

8. The sum of the ECL energy of tracks and clusters not associated with the signal B decay.
9. A set of variables developed by CLEO [31] that characterize the momentum flow into concentric areas around the thrust axis of a reconstructed B candidate.

The NN outputs a single variable \mathcal{O} , for which larger values correspond to more signal-like events. To facilitate modeling of the distribution of \mathcal{O} with an analytic function, we require $\mathcal{O} > -0.6$ ($= \mathcal{O}_{\min}$) and transform \mathcal{O} to a new variable:

$$\mathcal{O}' = \log \left[\frac{\mathcal{O} - \mathcal{O}_{\min}}{\mathcal{O}_{\max} - \mathcal{O}} \right],$$

where \mathcal{O}_{\max} is the upper boundary of \mathcal{O} . The criterion on \mathcal{O}_{\min} reduces the background events by more than 75%, with a signal loss of only 4-5%.

We study the remaining background events using MC simulation for individual modes, with special attention paid to those that can mimic signal decays. Candidates arising from $B^0 \rightarrow J/\psi(\rightarrow \ell^+\ell^-)K^{*0}$ populate towards the negative side in ΔE and are suppressed with the requirement $\Delta E > -0.1$ GeV. The decay $B^+ \rightarrow \bar{D}^0(\rightarrow K^+\pi^-)\pi^+$ mimics $B^+ \rightarrow K^+\mu^+\mu^-$ when both pions are mis-identified as muons; to suppress this background, we apply a veto on the invariant mass of the K^+ and μ^- candidates: $M[K^+\mu^-] \notin (1.85, 1.88)$ GeV/ c^2 . The contribution from other $B \rightarrow$ charm decays is negligible. Events originating from the decays $B^+ \rightarrow J/\psi(\rightarrow \mu^+\mu^-)K^+$, in which one of the muons is misidentified as a kaon and vice versa, contribute as a peaking background to $B^+ \rightarrow K^+\mu^+\mu^-$. Such events are suppressed by applying a veto on the invariant mass $M[K^+\mu^-] \notin (3.06, 3.13)$ GeV/ c^2 .

For the LFV modes, the background coming from $B^+ \rightarrow J/\psi(\rightarrow e^+e^-)K^+$ because of misidentification and swapping between particles is removed by invariant mass vetoes. For the $B^+ \rightarrow K^+\mu^+e^-$ mode, two vetoes are applied: (a) the electron is misidentified as kaon and kaon as muon, and thus the veto on the kaon-electron invariant mass is $M[K^+e^-] \notin (2.95, 3.11)$ GeV/ c^2 ; and (b) the electron is misidentified as a muon, and thus the muon-electron mass veto is $M[\mu^+e^-] \notin (3.02, 3.12)$ GeV/ c^2 . For the $B^+ \rightarrow K^+\mu^-e^+$ channel, only the latter background is found and removed using $M[\mu^+e^-] \notin (3.02, 3.12)$ GeV/ c^2 . A small contribution from $B^+ \rightarrow \bar{D}^0(K^+\pi^-)\pi^+$ for these LFV modes, due to misidentification of pions as leptons, is removed by requiring $M[K^+\mu^-] \notin (1.85, 1.88)$ GeV/ c^2 . For the $B^0 \rightarrow K_S^0 \mu^+e^-$ mode, a background contribution from $B^0 \rightarrow J/\psi(\rightarrow e^+e^-)K_S^0$, where an electron is misreconstructed as a muon, is suppressed by requiring $M[\mu^+e^-] \notin (3.04, 3.12)$ GeV/ c^2 . When calculating invariant masses for these vetoes, the mass hypothesis for the misidentified particle is used. There is a small background from $B \rightarrow K\pi^+\pi^-$ decays in the $B^+ \rightarrow K^+\mu^+\mu^-$ (1.37 ± 0.03 events), $B^0 \rightarrow K_S^0 \mu^+\mu^-$ (0.17 ± 0.01 events), $B^+ \rightarrow K^+\mu^+e^-$ (0.16 ± 0.03 events), $B^+ \rightarrow K^+\mu^-e^+$ (0.14 ± 0.03 events), and $B^0 \rightarrow K_S^0 \mu^+e^-$ (0.14 ± 0.02 events) samples. This background is negligible in the $B^+ \rightarrow K^+e^+e^-$ and $B^0 \rightarrow K_S^0 e^+e^-$ samples. The mentioned yields of peaking charmless B backgrounds are estimated by considering all known intermediate resonances. To avoid biasing our re-

sults, all selection criteria are determined in a “blind” manner, *i.e.*, they are finalized before looking at data events in the signal region.

We determine the signal yields by performing a three-dimensional unbinned extended maximum-likelihood fit to the M_{bc} , ΔE , and \mathcal{O}' distributions in different q^2 bins. The fits are performed for each mode separately. The probability density functions (PDFs) used to model signal decays are as follows: for M_{bc} we use a Gaussian, for ΔE the sum of a Gaussian and a Crystal Ball function [32], and for \mathcal{O}' the sum of a Gaussian and an asymmetric Gaussian with a common mean. All signal shape parameters are obtained from MC simulation. To account for small differences observed between data and MC simulations, we introduce an offset in the mean positions and scaling factors for the widths. The values of these parameters are obtained from fitting the control sample $B \rightarrow J/\psi(\rightarrow \ell^+\ell^-)K$ decays and kept fixed. The PDFs used for charmless $B \rightarrow K\pi^+\pi^-$ peaking background is the same as that of the signal PDFs, with the fixed number of peaking events. The shapes of the M_{bc} , ΔE , and \mathcal{O}' distributions for background arising from B decays are parameterized with an ARGUS function [33], an exponential, and a Gaussian function, respectively. Similarly, the continuum background is modeled using an ARGUS, a first-order polynomial, and a Gaussian function. The shapes of $B\bar{B}$ and continuum backgrounds are very similar in two of the fit variables, making it difficult to simultaneously float the yields of both backgrounds. Hence, the continuum yields are obtained for each mode from the off-resonance data sample and fixed in the fit. These yields are consistent with those of the high-statistics off-resonance MC sample. The $B\bar{B}$ yields are floated in the fit.

4 Results

The results of the fit projected into a signal-enhanced region for M_{bc} [$|\Delta E| < 0.05$ GeV and $\mathcal{O}' \in (1.0, 8.0)$], ΔE [$M_{bc} \in (5.27, 5.29)$ GeV/ c^2 and $\mathcal{O}' \in (1.0, 8.0)$] and \mathcal{O}' [$M_{bc} \in (5.27, 5.29)$ GeV/ c^2 and $|\Delta E| < 0.05$ GeV] distributions in the data sample are shown in Figs. 1 and 2 for $B^+ \rightarrow K^+\ell^+\ell^-$ and $B^0 \rightarrow K_s^0\ell^+\ell^-$, respectively. These distributions correspond to the whole q^2 ; $q^2 \in [(0.1, 8.75)(10.2, 13)(> 14.18)]$ GeV $^2/c^4$ with muon and $q^2 \in [(0.1, 8.12)(10.2, 12.8)(> 14.18)]$ GeV $^2/c^4$ with electron, in the final states.

There are 137 ± 14 and 138 ± 15 signal events for the decays $B^+ \rightarrow K^+\mu^+\mu^-$ and $B^+ \rightarrow K^+e^+e^-$, respectively, whereas the yields for the decays $B^0 \rightarrow K_s^0\mu^+\mu^-$ and $B^0 \rightarrow K_s^0e^+e^-$ are $27.3^{+6.6}_{-5.8}$ and $21.8^{+7.0}_{-6.1}$ events, respectively. The fit is also performed in the aforementioned five q^2 bins [(0.1, 4.0), (4.0, 8.12), (1.0, 6.0), (10.2, 12.8), and (> 14.18)] GeV $^2/c^4$ including the (1.0, 6.0) GeV $^2/c^4$ bin, where LHCb reports a possible deviation in R_{K^+} , and R_K and A_I values are calculated from Eqs. (1.1) and (1.2), respectively. The results are listed in Table 1 and R_K and A_I are also shown in Figs. 3 and 4, respectively. The differential branching fraction ($d\mathcal{B}/dq^2$) results are shown in Fig. 5. The branching fractions for the $B^+ \rightarrow K^+\ell^+\ell^-$, and $B^0 \rightarrow K^0\ell^+\ell^-$ modes are $(5.99^{+0.45}_{-0.43} \pm 0.14) \times 10^{-7}$, and $(3.51^{+0.69}_{-0.60} \pm 0.10) \times 10^{-7}$, respectively for the whole q^2 range. The measurement is done for $B^0 \rightarrow K_s^0\ell^+\ell^-$, but the branching fraction is quoted for $B^0 \rightarrow K^0\ell^+\ell^-$, considering a factor of 2. Figure 6 illustrates the fit for $B \rightarrow J/\psi(\rightarrow \ell^+\ell^-)K$ modes and the corresponding branching fractions obtained are listed in Table 2. Those samples serve as

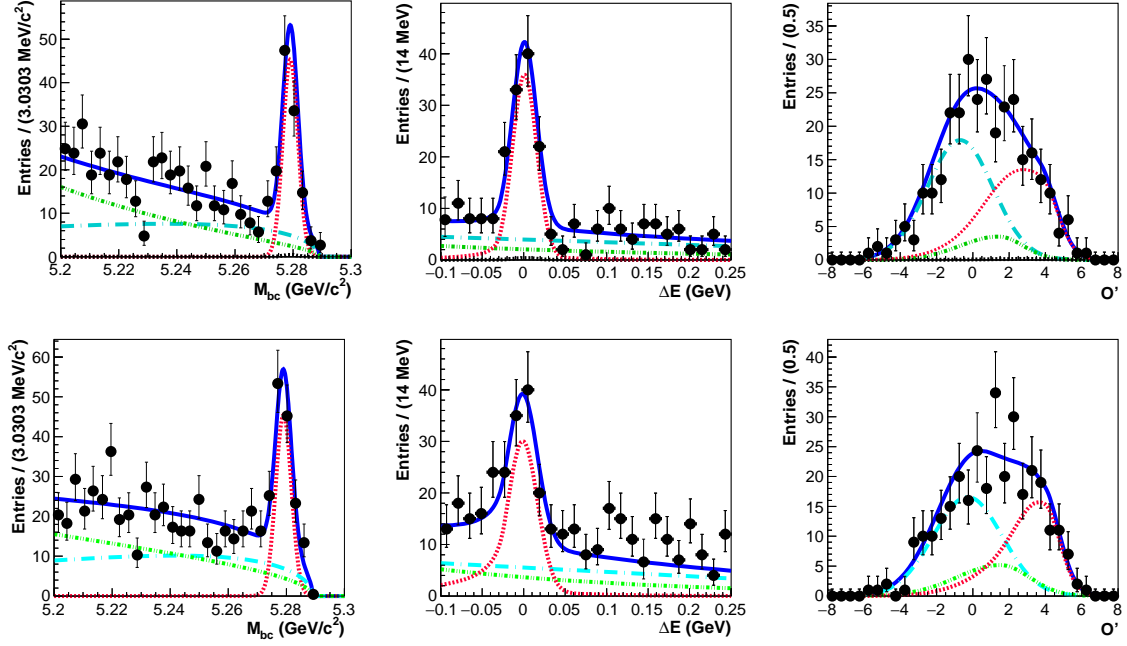


Figure 1. Signal-enhanced M_{bc} (left), ΔE (middle), and \mathcal{O}' (right) projections of three-dimensional unbinned extended maximum-likelihood fits to the data events that pass the selection criteria for $B^+ \rightarrow K^+ \mu^+ \mu^-$ (top), and $B^+ \rightarrow K^+ e^+ e^-$ (bottom). Points with error bars are the data; blue solid curves are the fitted results for the signal-plus-background hypothesis; red dashed curves denote the signal component; cyan long dashed, green dash-dotted, and black dashed curves represent continuum, $B\bar{B}$ background, and $B \rightarrow$ charmless decays, respectively.

calibration modes for the PDF shapes used, as well as to verify that there is no bias for some of the key observables. For example, we obtain $R_K(J/\psi) = 0.994 \pm 0.011 \pm 0.010$ and $0.993 \pm 0.015 \pm 0.010$ for $B^+ \rightarrow J/\psi K^+$ and $B \rightarrow J/\psi K_S^0$, respectively. Similarly, $A_I(B \rightarrow J/\psi K)$ is $-0.002 \pm 0.006 \pm 0.014$.

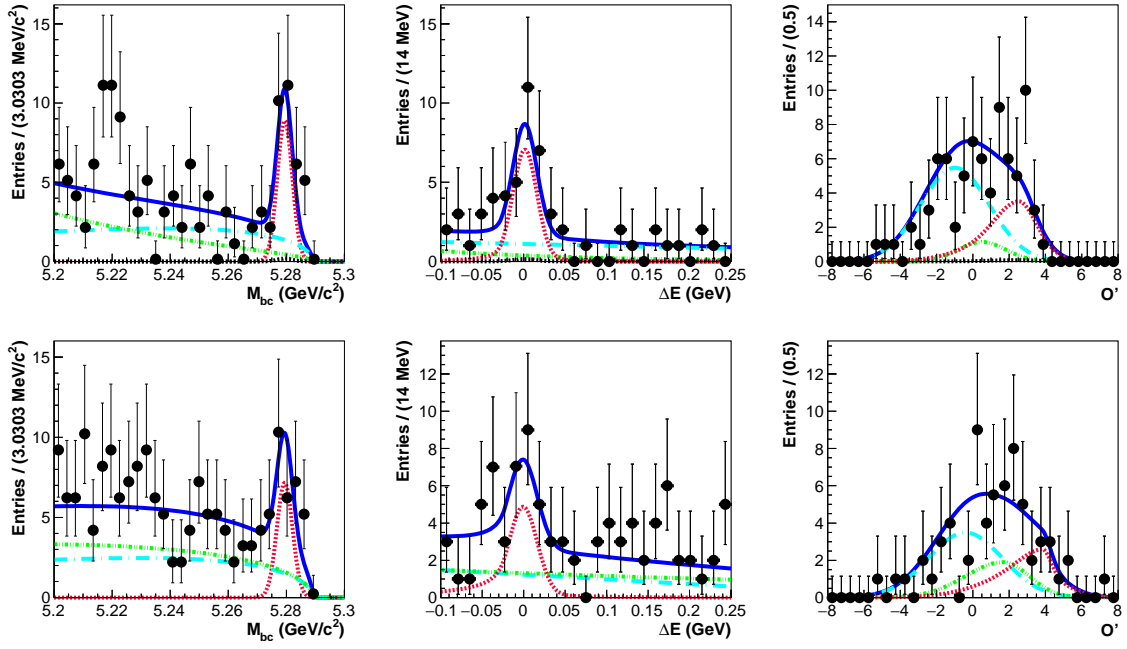


Figure 2. Signal-enhanced M_{bc} (left), ΔE (middle), and \mathcal{O}' (right) projections of three-dimensional unbinned extended maximum-likelihood fits to the data events that pass the selection criteria for $B^0 \rightarrow K_s^0 \mu^+ \mu^-$ (top), and $B^0 \rightarrow K_s^0 e^+ e^-$ (bottom). The legends are the same as in Fig. 1.

Table 1. Results from the fits. The columns correspond to the q^2 bin size, decay mode, reconstruction efficiency, signal yield, branching fraction, lepton-flavor-separated and combined A_I and R_K .

q^2 (GeV ² /c ⁴)	$B \rightarrow$ mode	ε (%)	N_{sig}	\mathcal{B} (10 ⁻⁷)	A_I (individual)	A_I (combined)	R_K (individual)	R_K (combined)
(0.1,4.0)	$K^+ \mu^+ \mu^-$	20.4	$28.4^{+6.6}_{-5.9}$	$1.76^{+0.41}_{-0.37} \pm 0.04$	$A_I(\mu\mu) =$	$-0.22^{+0.14}_{-0.12} \pm 0.01$	$R_{K^+} =$	$1.01^{+0.28}_{-0.25} \pm 0.02$
	$K_S^0 \mu^+ \mu^-$	14.7	$6.8^{+3.3}_{-2.6}$	$0.62^{+0.30}_{-0.23} \pm 0.02$	$-0.11^{+0.20}_{-0.17} \pm 0.01$		$0.98^{+0.29}_{-0.26} \pm 0.02$	
	$K^+ e^+ e^-$	29.1	$41.5^{+7.7}_{-7.0}$	$1.80^{+0.33}_{-0.30} \pm 0.05$	$A_I(ee) =$		$R_{K_S^0} =$	
	$K_S^0 e^+ e^-$	19.3	$5.5^{+3.6}_{-2.7}$	$0.38^{+0.25}_{-0.19} \pm 0.01$	$-0.35^{+0.21}_{-0.17} \pm 0.01$		$1.62^{+1.31}_{-1.01} \pm 0.02$	
(4.00,8.12)	$K^+ \mu^+ \mu^-$	29.0	$28.4^{+6.4}_{-5.7}$	$1.24^{+0.28}_{-0.25} \pm 0.03$	$A_I(\mu\mu) =$	$-0.09^{+0.15}_{-0.12} \pm 0.01$	$R_{K^+} =$	$0.85^{+0.30}_{-0.24} \pm 0.01$
	$K_S^0 \mu^+ \mu^-$	21.0	$4.2^{+4.2}_{-3.5}$	$0.27^{+0.18}_{-0.13} \pm 0.01$	$-0.34^{+0.23}_{-0.19} \pm 0.01$		$1.29^{+0.44}_{-0.39} \pm 0.02$	
	$K^+ e^+ e^-$	35.4	$26.9^{+6.9}_{-6.1}$	$0.96^{+0.24}_{-0.22} \pm 0.03$	$A_I(ee) =$		$R_{K_S^0} =$	
	$K_S^0 e^+ e^-$	23.9	$9.3^{+3.7}_{-3.0}$	$0.52^{+0.21}_{-0.17} \pm 0.02$	$0.10^{+0.20}_{-0.16} \pm 0.01$		$0.51^{+0.41}_{-0.31} \pm 0.01$	
(1.0,6.0)	$K^+ \mu^+ \mu^-$	23.2	$42.3^{+7.6}_{-6.9}$	$2.30^{+0.41}_{-0.38} \pm 0.05$	$A_I(\mu\mu) =$	$-0.31^{+0.13}_{-0.11} \pm 0.01$	$R_{K^+} =$	$1.03^{+0.28}_{-0.24} \pm 0.01$
	$K_S^0 \mu^+ \mu^-$	16.8	$3.9^{+2.7}_{-2.0}$	$0.31^{+0.22}_{-0.16} \pm 0.01$	$-0.53^{+0.20}_{-0.17} \pm 0.02$		$1.39^{+0.36}_{-0.33} \pm 0.02$	
	$K^+ e^+ e^-$	31.7	$41.7^{+8.0}_{-7.2}$	$1.66^{+0.32}_{-0.29} \pm 0.04$	$A_I(ee) =$		$R_{K_S^0} =$	
	$K_S^0 e^+ e^-$	21.1	$8.9^{+4.0}_{-3.2}$	$0.56^{+0.25}_{-0.20} \pm 0.02$	$-0.13^{+0.18}_{-0.15} \pm 0.01$		$0.55^{+0.46}_{-0.34} \pm 0.01$	
(10.2,12.8)	$K^+ \mu^+ \mu^-$	35.6	$24.3^{+6.3}_{-5.5}$	$0.86^{+0.22}_{-0.20} \pm 0.02$	$A_I(\mu\mu) =$	$-0.18^{+0.22}_{-0.18} \pm 0.01$	$R_{K^+} =$	$1.97^{+1.03}_{-0.89} \pm 0.02$
	$K_S^0 \mu^+ \mu^-$	26.5	$5.7^{+3.4}_{-2.6}$	$0.29^{+0.17}_{-0.13} \pm 0.01$	$-0.14^{+0.24}_{-0.19} \pm 0.01$		$1.96^{+1.03}_{-0.89} \pm 0.02$	
	$K^+ e^+ e^-$	40.3	$14.0^{+6.4}_{-5.5}$	$0.44^{+0.20}_{-0.17} \pm 0.01$	$A_I(ee) =$		$R_{K_S^0} =$	
	$K_S^0 e^+ e^-$	26.5	$1.1^{+3.7}_{-3.0}$	$0.06^{+0.19}_{-0.15} \pm 0.01$	$-0.55^{+0.73}_{-0.60} \pm 0.01$		$5.18^{+17.69}_{-14.32} \pm 0.06$	
> 14.18	$K^+ \mu^+ \mu^-$	45.2	$47.9^{+8.6}_{-7.8}$	$1.34^{+0.24}_{-0.22} \pm 0.03$	$A_I(\mu\mu) =$	$-0.14^{+0.14}_{-0.12} \pm 0.01$	$R_{K^+} =$	$1.16^{+0.30}_{-0.27} \pm 0.01$
	$K_S^0 \mu^+ \mu^-$	25.7	$9.6^{+4.2}_{-3.5}$	$0.49^{+0.22}_{-0.18} \pm 0.01$	$-0.08^{+0.17}_{-0.15} \pm 0.01$		$1.13^{+0.31}_{-0.28} \pm 0.01$	
	$K^+ e^+ e^-$	46.2	$43.2^{+9.1}_{-8.3}$	$1.18^{+0.25}_{-0.22} \pm 0.03$	$A_I(ee) =$		$R_{K_S^0} =$	
	$K_S^0 e^+ e^-$	24.9	$5.9^{+4.0}_{-3.1}$	$0.32^{+0.21}_{-0.17} \pm 0.01$	$-0.24^{+0.23}_{-0.19} \pm 0.01$		$1.57^{+1.28}_{-1.00} \pm 0.02$	
whole q^2	$K^+ \mu^+ \mu^-$	27.8	$137.0^{+14.2}_{-13.5}$	$6.24^{+0.65}_{-0.61} \pm 0.16$	$A_I(\mu\mu) =$	$-0.19^{+0.07}_{-0.06} \pm 0.01$	$R_{K^+} =$	$1.10^{+0.16}_{-0.15} \pm 0.02$
	$K_S^0 \mu^+ \mu^-$	18.5	$27.3^{+6.6}_{-5.9}$	$1.97^{+0.48}_{-0.42} \pm 0.06$	$-0.16^{+0.09}_{-0.08} \pm 0.01$		$1.08^{+0.16}_{-0.15} \pm 0.02$	
	$K^+ e^+ e^-$	30.3	$138.0^{+15.5}_{-14.7}$	$5.75^{+0.64}_{-0.61} \pm 0.15$	$A_I(ee) =$		$R_{K_S^0} =$	
	$K_S^0 e^+ e^-$	19.0	$21.8^{+7.0}_{-6.1}$	$1.53^{+0.49}_{-0.43} \pm 0.04$	$-0.24^{+0.11}_{-0.10} \pm 0.01$		$1.29^{+0.52}_{-0.45} \pm 0.01$	

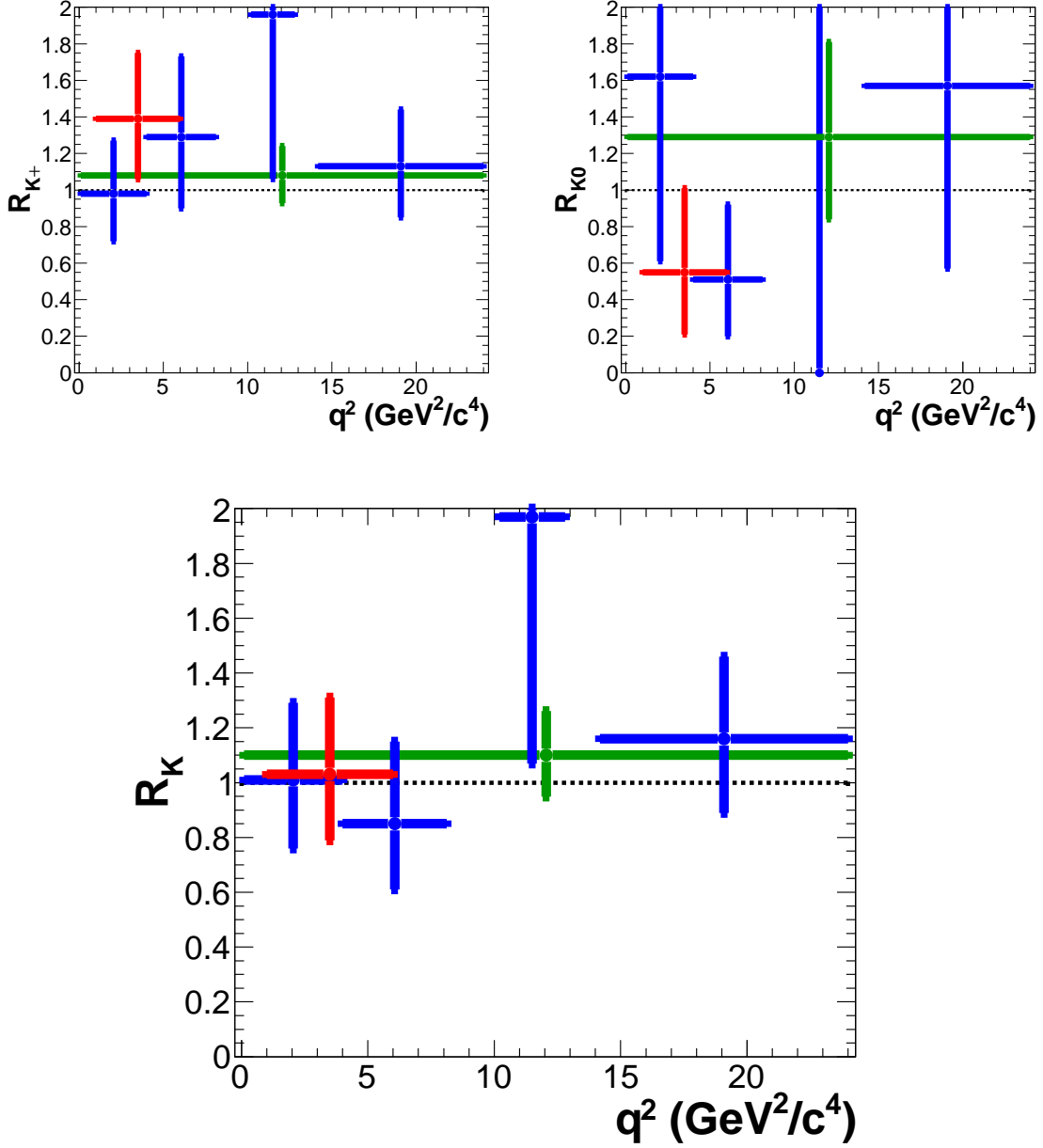


Figure 3. R_K in bins of q^2 , for $B^+ \rightarrow K^+ \ell^+ \ell^-$ (top-left), $B^0 \rightarrow K_S^0 \ell^+ \ell^-$ (top-right), and both modes combined (bottom). The red marker represents the bin of $1 < q^2 < 6$ GeV^2/c^4 , and the blue markers are for $0.1 < q^2 < 4$, $4 < q^2 < 8.12$, $10.2 < q^2 < 12.8$ and $q^2 > 14.18$ GeV^2/c^4 bins. The green marker denotes the whole q^2 region excluding the charmonium resonances.

The signal yields for LFV decays are obtained by performing unbinned extended maximum-likelihood fits, similar to those for the $B \rightarrow K \ell^+ \ell^-$ modes. The signal-enhanced projection plots with fit results for LFV decays are shown in Fig.7. The fitted yields are $11.6^{+6.1}_{-5.5}$, $1.7^{+3.6}_{-2.2}$, and $-3.3^{+4.0}_{-2.8}$ for $B^+ \rightarrow K^+ \mu^+ e^-$, $B^+ \rightarrow K^+ \mu^- e^+$, and $B^0 \rightarrow K_S^0 \mu^\pm e^\mp$, respectively. For the $B^0 \rightarrow K_S^0 \mu^\pm e^\mp$ modes, we consider $\mathcal{B}(B^0 \rightarrow K_S^0 \mu^+ e^-)$ and $\mathcal{B}(B^0 \rightarrow K_S^0 \mu^- e^+)$

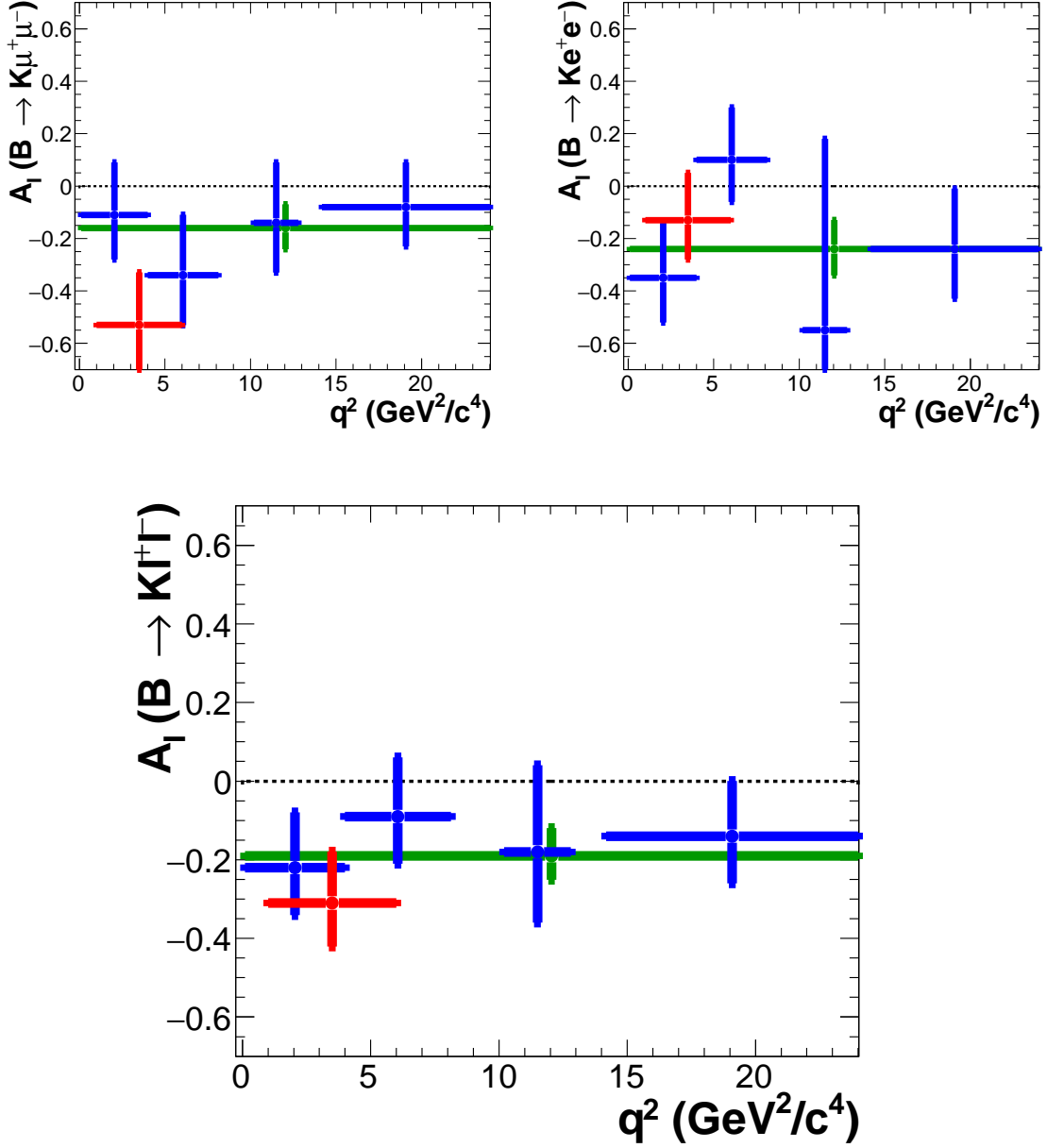


Figure 4. A_I measurements in bins of q^2 , for decays $B \rightarrow K\mu^+\mu^-$ (top-left), $B \rightarrow Ke^+e^-$ (top-right), and both modes combined (bottom). The legends are the same as in Fig. 3.

together, as we do not distinguish between B^0 and \bar{B}^0 . The total branching fraction $\mathcal{B}(B^0 \rightarrow K^0\mu^\pm e^\mp)$ corresponds, via isospin invariance, to $\mathcal{B}(B^+ \rightarrow K^+\mu^+e^-) + \mathcal{B}(B^+ \rightarrow K^+\mu^-e^+)$. The significance of the signal yield for $B^+ \rightarrow K^+\mu^+e^-$ channel is 3.2σ considering statistical and systematic uncertainties, while other modes are consistent with zero signal yield. The evidence for the signal is driven by one event. The significance is estimated with $\sqrt{-2\ln(\mathcal{L}_0/\mathcal{L}_{\max})}$, where \mathcal{L}_0 is the likelihood when N_{sig} is constrained to 0 and \mathcal{L}_{\max} is the likelihood of the nominal fit. To include the systematic uncertainty in significance,

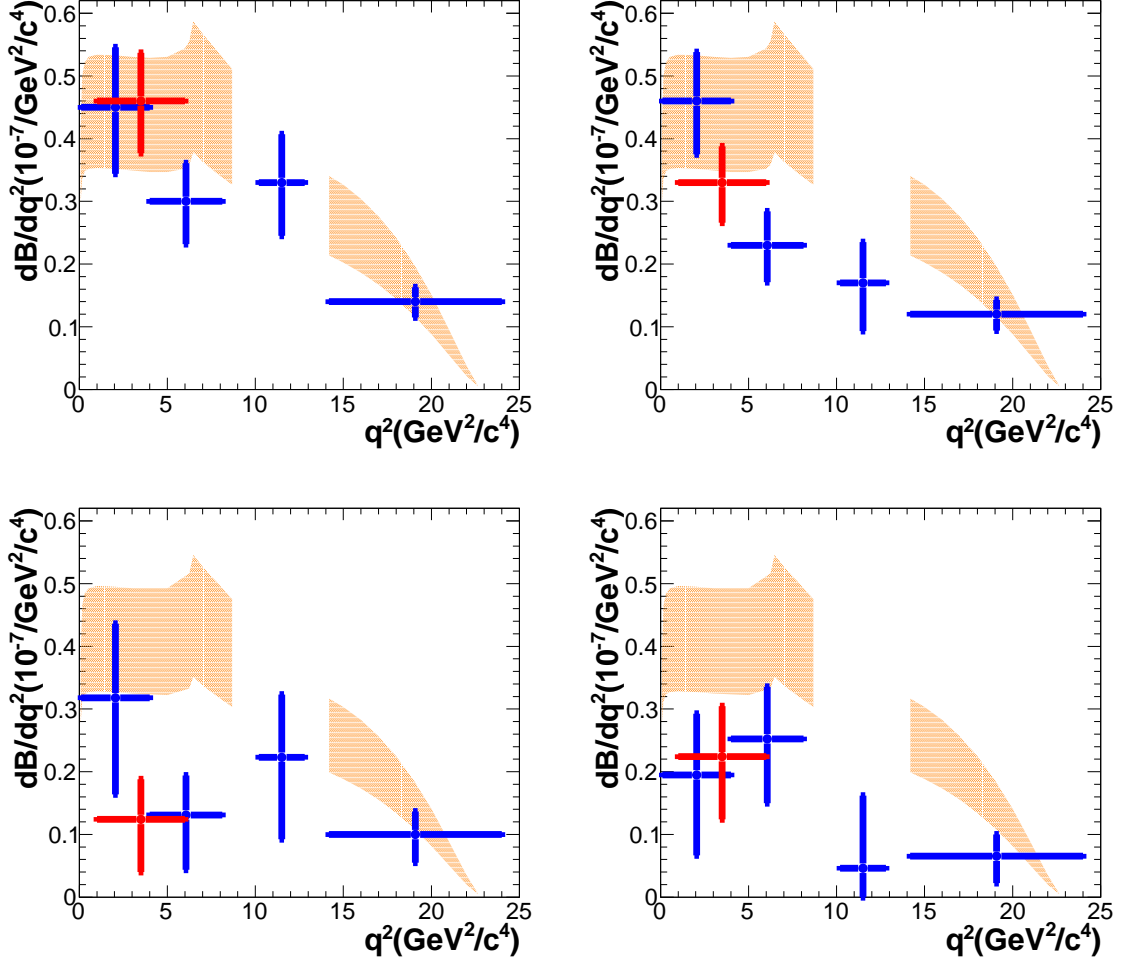


Figure 5. $d\mathcal{B}/dq^2$ measurements in bins of q^2 , for decays $B^+ \rightarrow K^+\mu^+\mu^-$ (top-left), $B^+ \rightarrow K^+e^+e^-$ (top-right), $B^0 \rightarrow K^0\mu^+\mu^-$ (bottom-left), and $B^0 \rightarrow K^0e^+e^-$ (bottom-right). The legends are the same as in Fig. 3. The yellow shaded regions show the theoretical predictions from the light-cone sum rule and lattice QCD calculations [37, 38].

Table 2. Branching fraction for $B \rightarrow K\ell^+\ell^-$ and $B \rightarrow J/\psi K$ decays.

Mode	\mathcal{B}
$B^+ \rightarrow K^+\ell^+\ell^-$	$(5.99^{+0.45}_{-0.43} \pm 0.14) \times 10^{-7}$
$B^0 \rightarrow K^0\ell^+\ell^-$	$(3.51^{+0.69}_{-0.60} \pm 0.10) \times 10^{-7}$
$B^+ \rightarrow J/\psi K^+$	$(1.032 \pm 0.007 \pm 0.024) \times 10^{-3}$
$B^0 \rightarrow J/\psi K^0$	$(0.902 \pm 0.010 \pm 0.026) \times 10^{-3}$

a Gaussian with width corresponding to the systematic uncertainty is convolved to the likelihood. We calculate the upper limit for these modes at 90% CL using a frequentist

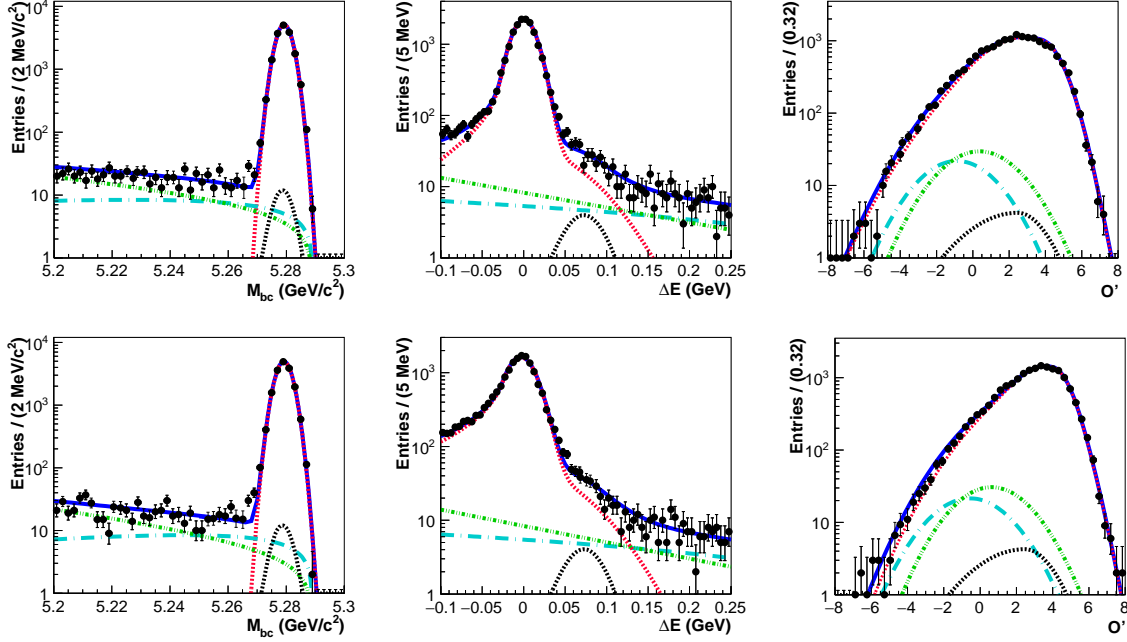


Figure 6. M_{bc} (left), ΔE (middle), and \mathcal{O}' (right) projections of three-dimensional unbinned extended maximum-likelihood fits to the data events that pass the selection criteria for $B^+ \rightarrow J/\psi(\rightarrow \mu^+\mu^-)K^+$ (top), and $B^+ \rightarrow J/\psi(\rightarrow e^+e^-)K^+$ (bottom). The legends are the same as in Fig. 1 and black dashed curve is $[\pi^+ J/\psi]$ background.

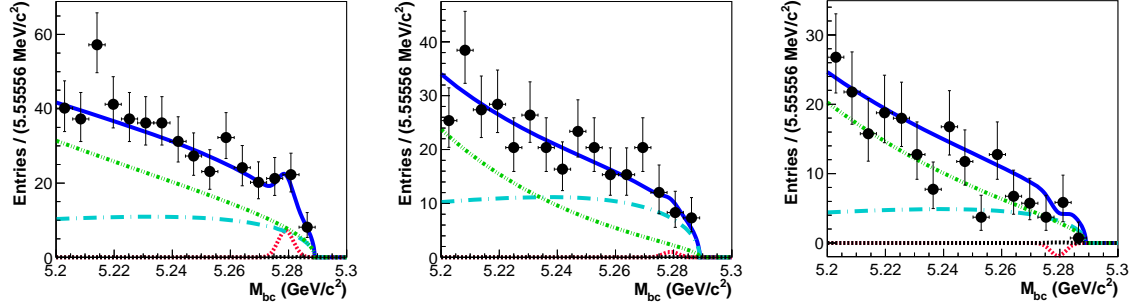


Figure 7. Signal-enhanced M_{bc} projection of three-dimensional unbinned extended maximum-likelihood fits to the data events that pass the selection criteria for decays $B^+ \rightarrow K^+\mu^+e^-$ (left), $B^+ \rightarrow K^+\mu^-e^+$ (middle), and $B^0 \rightarrow K_s^0\mu^\pm e^\mp$ (right). The legends are same as in Fig. 1.

method. In this method, for different numbers of signal events $N_{\text{sig}}(\text{gen})$, we generate 1000 Monte Carlo experiments with signal and background PDFs, with each set of events being statistically equivalent to our data sample of 711 fb^{-1} . We fit all these simulated data sets, and, for each value of $N_{\text{sig}}(\text{gen})$, we calculate the fraction of MC experiments that have $N_{\text{sig}} \leq N_{\text{sig}}(\text{data})$. The 90% CL upper limit is taken to be the value of $N_{\text{sig}}(\text{gen})$ (called here $N_{\text{sig}}^{\text{UL}}$) for which 10% of the experiments have $N_{\text{sig}} \leq N_{\text{sig}}(\text{data})$. The upper limit on the branching fraction is then derived using the formula:

$$\mathcal{B}^{\text{UL}} = \frac{N_{\text{sig}}^{\text{UL}}}{N_{B\bar{B}} \times 2 \times f^{+- (00)} \times \varepsilon},$$

where $N_{B\bar{B}}$ is the number of $B\bar{B}$ pairs $= (772 \pm 11) \times 10^6$, $f^{+- (00)}$ is the branching fraction $\mathcal{B}[\Upsilon(4S) \rightarrow B^+ B^-]$ ($\mathcal{B}[\Upsilon(4S) \rightarrow B^0 \bar{B}^0]$) for charged (neutral) B decays, and ε is the signal reconstruction efficiency calculated from signal MC samples. The systematic uncertainty in \mathcal{B}^{UL} is included by smearing the N_{sig} obtained from the MC fits with the fractional systematic uncertainty (discussed in Section 5). The results are listed in Table 3. As we observe non-negligible signal events in the LFV $B^+ \rightarrow K^+ \mu^+ e^-$ decay, in addition to reporting an upper limit we also provide the branching fraction to be $(5.0_{-2.4}^{+2.6} \pm 0.1) \times 10^{-8}$ for this decay.

Table 3. Branching fraction UL calculation at 90% CL for LFV $B \rightarrow K\mu e$ decays.

Mode	ε (%)	N_{sig}	$N_{\text{sig}}^{\text{UL}}$	$\mathcal{B}^{(\text{UL})}$ (10^{-8})
$B^+ \rightarrow K^+ \mu^+ e^-$	29.4	$11.6_{-5.5}^{+6.1}$	19.9	8.5
$B^+ \rightarrow K^+ \mu^- e^+$	31.2	$1.7_{-2.2}^{+3.6}$	7.5	3.0
$B^0 \rightarrow K^0 \mu^\pm e^\mp$	20.9	$-3.3_{-2.8}^{+4.0}$	3.0	3.8

5 Systematic uncertainties

Systematic uncertainties arising due to lepton identification is 0.3% (0.4%) for each muon (electron) selection. This uncertainty is calculated using an inclusive $J/\psi \rightarrow \ell^+ \ell^-$, $\ell = e$ or μ sample. Uncertainty due to hadron identification is 0.8% for K^+ using $D^{*+} \rightarrow D^0(K^-\pi^+)\pi^+$ sample and 1.6% for K_s^0 [34]. The systematic uncertainty due to charged track reconstruction is 0.35% per track estimated by using the partially reconstructed $D^{*-} \rightarrow \bar{D}^0\pi^-$, $\bar{D}^0 \rightarrow \pi^+\pi^-K_s^0$, and $K_s^0 \rightarrow \pi^+\pi^-$ events. The uncertainty in efficiency due to limited MC statistics is about 0.2%, and the uncertainty in the number of $B\bar{B}$ events is 1.4%. The systematic uncertainty in the branching fraction $\mathcal{B}[\Upsilon(4S) \rightarrow B^+ B^-]$ ($\mathcal{B}[\Upsilon(4S) \rightarrow B^0 \bar{B}^0]$) is 1.2% [9]. We compare the efficiency of the $\mathcal{O} > \mathcal{O}_{\text{min}}$ criterion between data and MC samples with the control channel $B \rightarrow J/\psi K$, $J/\psi \rightarrow \ell^+ \ell^-$; the differences between data and MC simulation (0.9-1.2%) are corrected and the corresponding uncertainty (0.2-0.3%) is assigned as a systematic uncertainty. The uncertainty due to PDF shapes is evaluated by varying the fixed shape parameters by $\pm 1\sigma$ and repeating the fit; the change in the central value of N_{sig} is taken as the systematic uncertainty, which ranges from 0.1 to 0.6%. The uncertainty due to the fixed yield of continuum events is estimated by varying the yield by $\pm 1\sigma$ in the fit; the resulting variation in N_{sig} is less than 1%. The charmless $B \rightarrow K\pi^+\pi^-$ background fixed in the fit for the modes with muon final states is varied within $\pm 1\sigma$ in the fit, and the change in N_{sig} is assigned as systematic, which is 0.1-0.2%. The decay model systematic for $B \rightarrow K\ell^+\ell^-$ modes is evaluated by comparing reconstruction efficiencies calculated from MC samples generated with different models [35, 36] and is 0.3 to 2.0% depending on the q^2 bin. For the $B \rightarrow J/\psi K$ branching fraction, we have considered all the sources except for the contribution due to

fixed continuum or charmless $B \rightarrow K\pi^+\pi^-$ events and the decay model. The systematic uncertainties such as hadron identification, track reconstruction, number of $B\bar{B}$ events, and the ratio $\mathcal{B}[\Upsilon(4S) \rightarrow B^+B^-]$ ($\mathcal{B}[\Upsilon(4S) \rightarrow B^0\bar{B}^0]$) cancel out in the double ratio of $R_K(J/\psi)$, while for $A_I(J/\psi K)$ the sources that divide out are lepton identification and number of $B\bar{B}$ events as listed in Table 4. In the case of R_K , systematic uncertainties due to hadron identification, charged track reconstruction, number of $B\bar{B}$ events, and the $\mathcal{B}[\Upsilon(4S) \rightarrow B^+B^-]$ ($\mathcal{B}[\Upsilon(4S) \rightarrow B^0\bar{B}^0]$) cancel, while for the A_I measurement lepton identification and the number of $B\bar{B}$ events cancel.

Table 4. Relative systematic uncertainties (%) for $\mathcal{B}(B \rightarrow J/\psi K)$, $R_K(J/\psi)$, and absolute uncertainty for $A_I(B \rightarrow J/\psi K)$.

Sources	$B^+ \rightarrow J/\psi K^+$	$B^0 \rightarrow J/\psi K_S^0$	$R_{K^+}(J/\psi)$	$R_{K^0}(J/\psi)$	$A_I(J/\psi K)$
Lepton identification	± 0.68	± 0.68	± 0.97	± 0.97	—
Kaon identification	± 0.80	—	—	—	± 0.007
K_S^0 identification	—	± 1.57	—	—	± 0.002
Track reconstruction	± 1.05	± 1.40	—	—	± 0.002
Efficiency calculation	± 0.14	± 0.18	± 0.20	± 0.25	± 0.001
Number of $B\bar{B}$ pairs	± 1.40	± 1.40	—	—	—
$f^{+- (00)}$	± 1.20	± 1.20	—	—	± 0.012
\mathcal{O}_{\min}	± 0.16	± 0.28	± 0.24	± 0.39	± 0.001
PDF shape parameters	$+0.15$ -0.20	$+0.05$ -0.10	$+0.22$ -0.31	$+0.10$ -0.20	± 0.002
Total	± 2.38	± 2.90	$+1.05$ -1.07	$+1.08$ -1.09	± 0.014

6 Summary

In summary, we have measured the differential branching fractions, their ratios (R_K), and the CP -averaged isospin asymmetry (A_I) for the $B \rightarrow K\ell^+\ell^-$ decays as a function of q^2 . The branching fraction for $B \rightarrow K\ell^+\ell^-$ modes are

$$\begin{aligned}\mathcal{B}(B^+ \rightarrow K^+\ell^+\ell^-) &= (5.99_{-0.43}^{+0.45} \pm 0.14) \times 10^{-7}, \\ \mathcal{B}(B^0 \rightarrow K^0\ell^+\ell^-) &= (3.51_{-0.60}^{+0.69} \pm 0.10) \times 10^{-7}.\end{aligned}$$

The branching fraction for $B^+ \rightarrow J/\psi K^+$, and $B^0 \rightarrow J/\psi K^0$ are $(1.032 \pm 0.007 \pm 0.024) \times 10^{-3}$, and $(0.902 \pm 0.010 \pm 0.026) \times 10^{-3}$, respectively. The R_K values for different q^2 bins are consistent with the SM predictions, and the value for the whole q^2 range is $1.10_{-0.15}^{+0.16} \pm 0.02$. The results for five q^2 bins are

$$R_K = \begin{cases} 1.01_{-0.25}^{+0.28} \pm 0.02 & q^2 \in (0.1, 4.0) \text{ GeV}^2/c^4, \\ 0.85_{-0.24}^{+0.30} \pm 0.01 & q^2 \in (4.0, 8.12) \text{ GeV}^2/c^4, \\ 1.03_{-0.24}^{+0.28} \pm 0.01 & q^2 \in (1.0, 6.0) \text{ GeV}^2/c^4, \\ 1.97_{-0.89}^{+1.03} \pm 0.02 & q^2 \in (10.2, 12.8) \text{ GeV}^2/c^4, \\ 1.16_{-0.27}^{+0.30} \pm 0.01 & q^2 > 14.18 \text{ GeV}^2/c^4. \end{cases}$$

Our result of R_{K^+} for the bin of interest, $q^2 \in (1.0, 6.0) \text{ GeV}^2/c^4$, is higher than the LHCb result [6, 39] by 1.6σ . The A_I values for almost all the bins for different channels show a negative asymmetry. For the bin $q^2 \in (1.0, 6.0) \text{ GeV}^2/c^4$, the obtained A_I value deviates from zero by 2.6σ for the mode with muon final states. The A_I value for the whole q^2 range is $-0.19_{-0.06}^{+0.07} \pm 0.01$. We see no deviation in differential branching fractions for the mode $B^+ \rightarrow K^+ \mu \mu$, where LHCb [40] observes lower values than the standard model predictions. The values for this observable are lower than the theoretical prediction for neutral B decays, reflecting $A_I < 1$. We have also searched for the lepton-flavor-violating $B \rightarrow K \mu e$ decays and set upper limits on their branching fractions at 90% CL:

$$\begin{aligned}\mathcal{B}(B^+ \rightarrow K^+ \mu^+ e^-) &< 8.5 \times 10^{-8}, \\ \mathcal{B}(B^+ \rightarrow K^+ \mu^- e^+) &< 3.0 \times 10^{-8}, \\ \mathcal{B}(B^0 \rightarrow K^0 \mu^\pm e^\mp) &< 3.8 \times 10^{-8}.\end{aligned}$$

We improve the existing limit on the neutral decay mode by an order of magnitude. More precisely, the limit of BaBar [16] is 2.7×10^{-7} , *i.e.*, the improvement is by a factor of 7.1.

7 Acknowledgments

KT wishes to thank S. Descotes-Genon for useful discussions. We thank the KEKB group for the excellent operation of the accelerator; the KEK cryogenics group for the efficient operation of the solenoid; and the KEK computer group, and the Pacific Northwest National Laboratory (PNNL) Environmental Molecular Sciences Laboratory (EMSL) computing group for strong computing support; and the National Institute of Informatics, and Science Information NETwork 5 (SINET5) for valuable network support. We acknowledge support from the Ministry of Education, Culture, Sports, Science, and Technology (MEXT) of Japan, the Japan Society for the Promotion of Science (JSPS), and the Tau-Lepton Physics Research Center of Nagoya University; the Australian Research Council including grants DP180102629, DP170102389, DP170102204, DP150103061, FT130100303; Austrian Science Fund (FWF); the National Natural Science Foundation of China under Contracts No. 11435013, No. 11475187, No. 11521505, No. 11575017, No. 11675166, No. 11705209; Key Research Program of Frontier Sciences, Chinese Academy of Sciences (CAS), Grant No. QYZDJ-SSW-SLH011; the CAS Center for Excellence in Particle Physics (CCEPP); the Shanghai Pujiang Program under Grant No. 18PJ1401000; the Ministry of Education, Youth and Sports of the Czech Republic under Contract No. LTT17020; the Carl Zeiss Foundation, the Deutsche Forschungsgemeinschaft, the Excellence Cluster Universe, and the VolkswagenStiftung; the Department of Science and Technology of India; the Istituto Nazionale di Fisica Nucleare of Italy; National Research Foundation (NRF) of Korea Grants No. 2016R1D1A1B01010135, No. 2016R1D1A1B02012900, No. 2018R1A2B3003643, No. 2018R1A6A1A06024970, No. 2018R1D1A1B07047294, No. 2019K1A3A7A09033840; Radiation Science Research Institute, Foreign Large-size Research Facility Application Supporting project, the Global Science Experimental Data Hub Center of the Korea Institute of Science and Technology Information and KREONET/GLORIAD; the Polish Ministry of Science and Higher Education and the National Science Center; the Grant of the Russian

Federation Government, Agreement No. 14.W03.31.0026; the Slovenian Research Agency; Ikerbasque, Basque Foundation for Science, Spain; the Swiss National Science Foundation; the Ministry of Education and the Ministry of Science and Technology of Taiwan; and the United States Department of Energy and the National Science Foundation.

References

- [1] G. Hiller and F. Kruger, Phys. Rev. D **69**, 074020 (2004).
- [2] C. Bobeth, G. Hiller, and G. Piranishvili, J. High Energy Phys. **12**, 040 (2007).
- [3] M. Bauer and M. Neubert, Phys. Rev. Lett. **116**, 141802 (2016).
- [4] R. Aaij *et al.* (LHCb Collaboration), J. High Energy Phys. **08**, 055 (2017).
- [5] A. Abdesselam *et al.* (Belle Collaboration), arXiv:1904.02440
- [6] R. Aaij *et al.* (LHCb Collaboration), Phys. Rev. Lett. **122**, 191801 (2019).
- [7] J. T. Wei *et al.* (Belle Collaboration), Phys. Rev. Lett. **103**, 171801 (2009).
- [8] T. Feldmann and J. Matias, J. High Energy Phys. **01**, 074 (2003).
- [9] P. Zyla *et al.* (Particle Data Group), Prog. Theor. Exp. Phys. **2020**, 083C01 (2020).
- [10] J. Lyon and R. Zwicky, Phys. Rev. D **88**, 094004 (2013).
- [11] J. P. Lees *et al.* (BaBar Collaboration), Phys. Rev. D **86**, 032012 (2012).
- [12] R. Aaij *et al.* (LHCb Collaboration), J. High Energy Phys. **06**, 133 (2014).
- [13] S. L. Glashow, D. Guadagnoli, and K. Lane, Phys. Rev. Lett. **114**, 091801 (2015).
- [14] J. C. Helo, S. Kovalenko, and I. Schmidt, Nucl. Phys. **B853**, 80 (2011).
- [15] R. Aaij *et al.* (LHCb Collaboration), Phys. Rev. Lett **123**, 241802 (2019).
- [16] B. Aubert *et al.* (BaBar Collaboration), Phys. Rev. D **73**, 092001 (2006).
- [17] S. Kurokawa and E. Kikutani, Nucl. Instrum. Methods Phys. Res., Sec. A **499**, 1 (2003), and other papers included in this volume; T. Abe *et al.*, Prog. Theor. Exp. Phys. **2013**, 03A001 (2013) and following articles up to 03A011.
- [18] A. Abashian *et al.* (Belle Collaboration), Nucl. Instrum. Methods Phys. Res., Sec. A **479**, 117 (2002); also, see the detector section in J. Brodzicka *et al.*, Prog. Theor. Exp. Phys. **2012**, 04D001 (2012).
- [19] Z. Natkaniec *et al.* (Belle SVD2 Group), Nucl. Instrum. Methods Phys. Res., Sec. A **560**, 1 (2006).
- [20] D. J. Lange, Nucl. Instrum. Methods Phys. Res., Sec. A **462**, 152 (2001).
- [21] A. Ali, P. Ball, L. T. Handoko, and G. Hiller, Phys. Rev. D **61**, 074024 (2000).
- [22] E. Barberio and Z. W̑s, Comput. Phys. Commun. **79**, 291 (1994); P. Golonka and Z. W̑s, Eur. Phys. J. C **45**, 97 (2006); P. Golonka and Z. W̑s, Eur. Phys. J. C **50**, 53 (2007).
- [23] R. Brun *et al.*, CERN Report No. DD/EE/84-1 (1984).
- [24] The inclusion of the charge-conjugate decay mode is implied unless otherwise stated.
- [25] A. Abashian *et al.*, Nucl. Instrum. Methods Phys. Res., Sec. A **491**, 69 (2002).

- [26] E. Nakano, Nucl. Instrum. Methods Phys. Res., Sec. A **494**, 402 (2002).
- [27] K. Hanagaki, H. Kakuno, H. Ikeda, T. Iijima, and T. Tsukamoto, Nucl. Instrum. Methods Phys. Res., Sec. A **485**, 490 (2002).
- [28] S. H. Lee *et al.* (Belle Collaboration), Phys. Rev. Lett. **91**, 261801 (2003).
- [29] G. C. Fox and S. Wolfram, Phys. Rev. Lett. **41**, 1581 (1978).
- [30] H. Kakuno *et al.* (Belle Collaboration), Nucl. Instrum. Methods Phys. Res., Sec. A **533**, 516 (2004).
- [31] D. M. Asner *et al.* (CLEO Collaboration), Phys. Rev. D **53**, 1039 (1996).
- [32] T. Skwarnicki, Ph.D. thesis, Institute for Nuclear Physics, Krakow; DESY Internal Report No. DESY F31-86-02, 1986.
- [33] H. Albrecht *et al.* (ARGUS Collaboration), Phys. Lett. B **241**, 278 (1990).
- [34] N. Dash *et al.* (Belle Collaboration), Phys. Rev. Lett. **119**, 171801 (2017).
- [35] D. Melikhov *et al.*, Phys. Lett. B **410**, 290 (1997).
- [36] P. Colangelo *et al.*, Phys. Rev. D **53**, 3672 (1996).
- [37] C. Bobeth, G. Hiller, and D. van Dyk, J. High Energy Phys. **07**, 067 (2011).
- [38] C. Bobeth, G. Hiller, D. van Dyk, and C. Wacker, J. High Energy Phys. **01**, 107 (2012).
- [39] R. Aaij *et al.* (LHCb Collaboration), Phys. Rev. Lett. **113**, 151601 (2014).
- [40] R. Aaij *et al.* (LHCb Collaboration), J. High Energy Phys. **06**, 133 (2014).